Results in Engineering 23 (2024) 102833

Contents lists available at ScienceDirect

Results in Engineering

journal homepage: www.sciencedirect.com/journal/results-in-engineering

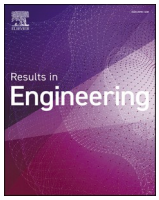

Parameter identification of thermoelectric modules using enhanced slime mould algorithm (ESMA)

Dharswini Ponnalagu, Mohd Ashraf Ahmad *, Julakha Jahan Jui

Faculty of Electrical and Electronics Engineering Technology, Universiti Malaysia Pahang Al-Sultan Abdullah, Malaysia

ARTICLE INFO

Keywords:
Thermoelectric modules
Parameter identification
Slime mould algorithm
Metaheuristics algorithms

ABSTRACT

This paper sets pioneering research which investigates the parametric identification of thermoelectric modules (TEMs) through the employment of enhanced slime mould algorithm (ESMA). The proposed method incorporates a pair of modifications to the standard slime mould algorithm (SMA). Primary modification encloses computation of random average position between the slimes' current individual position and best individual position towards resolution of local optima issue. Subsequent modification then involves substitution of an exponential function to the existing tangent hyperbolic function within formula *p* of the standard SMA in enabling improved probability variants via the selection of updated equations. Competency of the proposed algorithm in generating the optimal parameters for TEMs was appraised based on 21 benchmarked design parameters, following the objective of root mean square error (RMSE) minimization between the temperature of both actual and estimated models. Acquired results which demonstrate lower values of RMSE and parameter deviation index against the standard SMA and other preceding algorithms such as particle swarm optimization, sine cosine algorithm, moth flame optimizer and ant lion optimizer ultimately verified ESMA's efficacy as an effective approach for accurate model identification.

1. Introduction

Continuous demands for fossil fuels and refractory devastation of carbon deluge on the global scale have considerably synchronized the aspirations among communities and professionals alike towards the search for healthier and sustainable energy conversion alternatives. This is also in line with the 2030 Agenda of the United Nations (UN) revolves around the Sustainable Development Goals (SDGs) [1]. While viable options such as solar-, hydrokinetic-, thermal- and wind-powered applications have gained substantial efficiency since their initial commencements, several circumstances have, nonetheless, ensued lavish preservation costs. Such realization then steered partiality to small-scale electric power systems that capitalize proficient implementation at suburban or deserted territories where sustainable or alternative energy sources are commonly inadequate [2]. Amidst the wide varieties of large-scale energy conversion approaches, the prevalence of solid-state thermoelectric or TEMs, being a distinguished variant of small-scale electrical power systems, thus, surfaced as a transcending renewable and amiable energy source.

Reflected through the governance of adjustable temperature systems, the practicality and convenience of TEMs are lifted ensuring its modest mechanism with the absence of dynamic components. However, its robustness remains shadowed by the efficacies of routine electric coolers and generators. With this being said, the continuous decline in power usage and tangible appearance of present-day appliances have unearthed a multitude of technological upgrades with the like of modernized ultra-low voltage conversion, strategic thermal energy harvesting circuits for sensor system [3–5], as well as autonomous thermoelectric-based energizing gadgets. The precision of the TEMs model then emerged as the apex guideline in ensuring accurate temperature management towards thermal characterization [6,7]. TEMs' efficacy in energy harvesting, thus, fascinated practitioners and researchers from diverse sectors towards examining its modelling and definition.

The modelling efficacy of TEMs was explicitly acknowledged towards a vast span of actual and functional implementations. As exemplified through [8], implementation of TEMs as simulated for waste heat recovery of vehicle engine has especially eased the observation of transformations in engine speed and coolant temperature within the system's radiator through its well-refined modelling. Following

* Corresponding author.
E-mail addresses: dharswini97@gmail.com (D. Ponnalagu), mashraf@umpsa.edu.my (M.A. Ahmad), julakha.ump@gmail.com (J.J. Jui).

https://doi.org/10.1016/j.rineng.2024.102833
Received 13 July 2024; Received in revised form 25 August 2024; Accepted 2 September 2024
Available online 3 September 2024

behavioral inspection of TEMs from the outlook of automotive velocity by Ref. [9], excessive transformation in the driving cycles has been shown to inversely affect the model's effectiveness. Nevertheless, investigation of the TEMs model in the automotive sector was similarly executed within the studies by Refs. [10–12]. Additionally, both the temperature profiles and electrical output as retrievable from the conical nozzle of a helicopter with the employment of TEMs were also examined in Ref. [13]. Reputably, the model was further developed and studied within numerous other mechanical functions including biomass boiler [14], small-scale pellet boiler [15], marine waste incinerator [16], refineries, glass manufacturing and foundries, as well as diverse heated elements such as wood-burning stoves [17], geothermal, solar salt ponds and solar concentrators [18].

As observable via Fig. 1, TEMs fundamentally comprise N sets of semiconductors held between two ceramic plates. Given its primary intention for appropriate temperature profiling towards the interpretation of the analyzed material, fundamental emphasis on the development of an accurate temperature controller then urges a strategic blueprint that proximately replicates the natural demeanor of actual TEMs towards effective manipulation of temperature change. Two main modelling categories are particularly noted towards the identification of TEMs, which comprised non-parametric modelling that adopts minimalistic or zero pre-disclosed inferences regarding the model's layout, and parametric modelling that exploits any existing intelligence centering the model's structure. However, TEMs are deemed admirable for implementation of the latter, conforming to its vastly disclosed principle physical demeanor, whilst the availability of extensive information concerning the phenomenological models. Modern endeavors concerning the parametric modelling of TEMs in Refs. [19–21] further propelled the adoption of particle swarm optimization (PSO) as the metaheuristic algorithm apropos the input of excitation current and the output of temperature responses. Nevertheless, the setback of premature convergence which impairs the converged precision of the investigated PSO algorithm has blemished its excellence for resolution of otherwise complicated and multi-modal challenges. The discovery, thus, steered additional scouting of alternative metaheuristic approaches that avoid such deficiency.

Consideration is then shifted to the contemporary metaheuristic approach as formerly designed and introduced by Shimin Li [22] by the name of slime mould algorithm (SMA) for the identification of TEMs model. Driven by the circulated motions of slime mould, the algorithm possesses a novel arithmetical structure which demonstrates the propagation wave of slimes by incorporation of adaptive weights in creating the finest route to forage food. The algorithm has simultaneously gained far-reaching employment within multiple areas of the engineering sector for its compelling exploratory and exploitation competencies, encompassing the contexts of solar cell estimation [23], image segmentation [24], power system stabilizer [25], and parametric modification of support vector regression [26].

SMA further solidified its applicability to tackle the parametric identification of TEMs by exhibiting utmost optimization feasibility against other practical metaheuristic counterparts such as PSO, grey wolf optimizer (GWO) [27], bald eagle search (BES) [28], and moth flame optimization (MFO) [29] with generating the best solutions to the majority of the gauged itineraries and real-time engineering challenges. Whilst mirroring the nature of metaheuristic algorithms at large, limitations of the SMA layout are comparably hyped on its excessive potential for local optima entrapment contributed by several inadequacies. The primary drawback is essentially recognized on the overwhelming dependency of slime mould's positional updates via each iteration to the best individual position with the greatest concentration of odor. Performance debilitation ensues under the circumstance where surrounding slimes are guided by the trapped best individual position towards its stationed local optima region.

Additionally, the secondary drawback then acknowledges insufficiency in the layout of formula p from in (2.2) of [22] towards varied generations of applicable alternatives for positional updates of individual slime. Attention is allocated to the immense disparity between the slimes' individual fitness and best fitness with the pre-established p that rendered extreme reliance on their individual position to the best individual position. Rigorous examination and surmounting of such setbacks through the development and execution of an advanced SMA, therefore, emerged as a noteworthy topic. So far, there have been many modifications of SMA to solve the local entrapment problem and most of the enhanced versions are based on the combination of SMA with various existing metaheuristics algorithms, such as SMA-whale optimization algorithm (WOA) [30,31], SMA-Teaching–Learning-Based Optimization (TLBO) [32,33], and SMA-Differential Evolution (DE) [34]. However, these modifications are prone to introducing new challenges, such as increased complexity in tuning control parameters, elevated computational costs, a growing population size with advancing generations, an excessive number of algorithmic coefficients requiring determination, and slower convergence at the initial stages of iterations. Therefore, it is worthwhile to propose a new and enhanced version of the SMA, capable of addressing the primary issue of local entrapment with significantly reduced complexity, fewer coefficients to be determined, and lower computational costs.

With reference to the previous discussion, the enhanced slime mould algorithm (ESMA) has been particularly introduced within the current paper towards the identification of both fixed and active parameters of two embedded TEMs through the sole incorporation of temperature estimation. A pair of constructive alterations are hereby operationalized in resolving aforementioned shortcomings of the standard SMA. Such executions comprise deliberation of random average position between the slime mould's current individual position and best individual position for the most recent iteration, followed by substitution of an exponential function to the existing tangent hyperbolic function within formula p from (2.2). Reciprocated supports among current individual position and best individual position of included slimes towards promising withdrawal from the local optima and greater probability variations in the selection of revised equations in (2.2) of [22] are, therefore, expected to recede the overwhelming reliance of slimes' individual position update on the best individual position, whilst advancing the agents' exploratory capacity for contemporary search track. The adoption of assimilation between the current and best position is based on our previous works reported in Refs. [35–38] which have shown its effectiveness in solving the local optima entrapment issue. Moreover, it has been verified to solve diverse types of control engineering problems such as neuroendocrine PID [35] and fractional order PID [36] controller tuning, nonlinear system identification [37], and parameter identification of solar cells [38].

Accounting for the 21 parameters of TEMs concerning the given information on both input current and output temperature towards appraising optimization robustness of ESMA, suggested parametric identification hereby engages minimization of mean squares error between both temporal temperature responses of the estimated and the

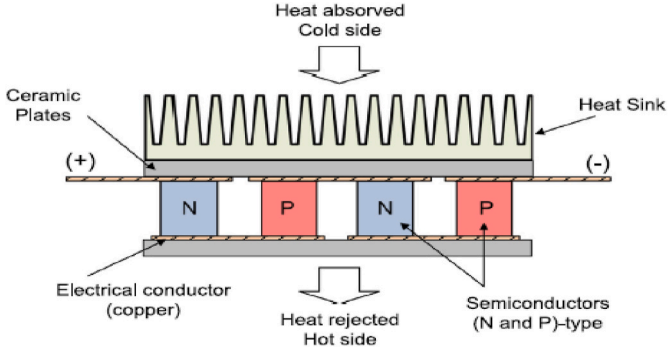

Fig. 1. Cross-sectional diagram of a TEM [19].

actual models. An objective function which gauges the root mean square error (RMSE) of the simulated temperature data to the identified temperature data has been specially employed in converting the previously determined estimation problem into an optimization problem, pending implementation of the proposed approach which centralizes minimization of RMSE towards attaining the optimal parameters of a TEMs model. Centralizing the minimization of RMSE, the practicability of the proposed approach would be appraised via components of plotted convergence curve for the objective function, parameter deviation index, as well as the aftereffects of time-domain output temperature between both simulated and identified data. Performance outcomes as recorded with the implementation of the ESMA-based method are subsequently measured against the results obtained from PSO, SMA, GWO, BES, and MFO-based methods. Thereafter, the current discovery would produce key contributions enclosing:

- A revolutionary variant of SMA known as the ESMA-based method has been spearheaded towards calibrating the 21 parameters of a TEMs model.
- A pair of modifications are pioneered towards resolving the setback of local optima entrapment within the standard SMA, enclosing the engagement of random average position between the slimes' current individual position and best individual position; followed by the substitution of an exponential function to formula p of SMA for allowing increased alternatives in the selection of revised equations. Prevailed as an advanced variant of SMA, ESMA indisputably possesses soaring potential in addressing polymorphic challenges as encountered within real-time engineering applications.
- In view of the parametric outcomes which hold the closest proximity to TEMs' optimal parameters, the operational excellence of ESMA is validated against its predecessor and other preceding optimization approaches. Proficiency of the proposed method towards steady and accurate estimations of TEMs' parameters is, therefore, confirmed.

A comprehensive rundown of the current paper is given as follows: Section 2 specifies the arithmetic modelling of TEMs, alongside a formulated problem concerning optimization of the system's parameters. Section 3 subsequently ensues with a brief explanation of the standard SMA. Following this, the contemporarily introduced ESMA-based method has been comprehensively described in Section 4 while emphasizing its functionality towards the optimization challenge of TEMs. Simulated findings as measured against the results from other existing algorithms are further demonstrated in Section 5 in validating the parametric robustness of the proposed method. This paper is ultimately wrapped through the concluding remarks as given in Section 6.

2. Mathematical model of TEMs and problem formulation

Arithmetic modelling of the TEMs system is particularly detailed within the current section in enabling problem formulation concerning the identification of the model's parameters. The research problem which sets to address the 21 parameters of TEMs model is fundamentally defined as appropriating the two embedded TEMs models of TEM_1 and TEM_2 as considered within the current study.

2.1. Mathematical model of TEMs apparatus

The currently investigated structure consisting of an interceding combination of two embedded TEMs alongside an analyzed medium has been comprehensively illustrated in Fig. 2. With robustness pertaining to a multitude of circumstances viz. humidity and temperature, the analyzed medium or material exclusively perchance a virtually replicated human skin towards integration of wearable thermoelectric generators (TEG). Such design further encompasses the components of TEM_1 junction, TEM_2 junction, a sensor and two heat sinks. Increased clarity on the proposed thermal structure is further displayed through

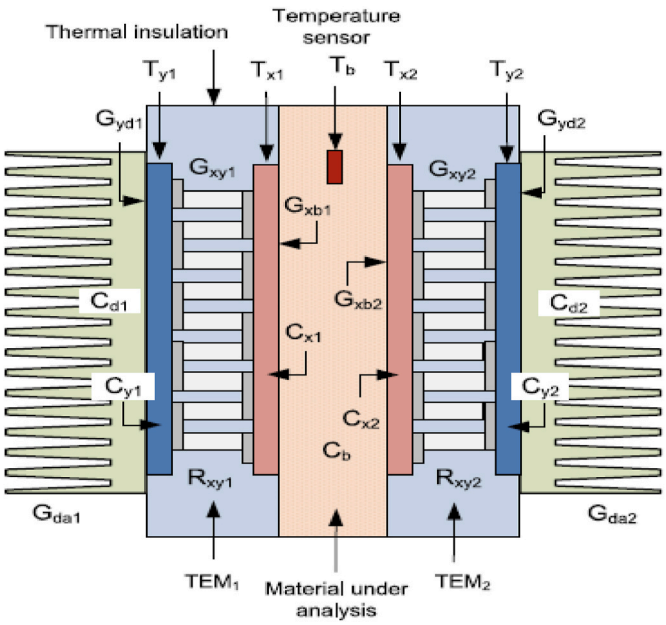

Fig. 2. The two embedded TEMs mechanical structure for parameter estimation [19].

the corresponding electrical equivalent model as demonstrated in Fig. 3, with thermal conductance between the heat sink and its surroundings being individually denoted by G_{da1} and G_{da2}, thermal conductance between the summit and nether sides of TEM_1 and TEM_2 being individually denoted by G_{xy1} and G_{xy2}, thermal conductance of the analyzed material being individually denoted by G_{xb1} and G_{xb2}, whilst thermal conductance between the heat sink and the nether sides of TEM_1 and TEM_2 are individually denoted by G_{yd1} and G_{yd2}, respectively.

The thermal capacitance of TEM_1, TEM_2 and the analyzed material is concurrently represented by the respective symbolic arrays of C_{d1}, C_{y1} and C_{x1}; C_{d2}, C_{y2} and C_{x2}; and C_b. The heat sink temperature of TEM_1 has been given by the symbol T_{d1}, whilst the temperature of the analyzed material is given by the symbol T_b, temperature at the summits of TEM_1 and TEM_2 being given by the independent symbols of T_{x1} and T_{x2}, room temperature as predetermined at 298 K being given by the independent symbols of T_{a1} and T_{a2}, and temperature at the nether sides of TEM_1 and TEM_2 being given by the independent symbols of T_{y1} and T_{y2}, respectively. Electrical resistors of both TEM_1 and TEM_2 are further represented by the independent symbols of R_{xy1} and R_{xy2}. Whereas, the voltage of the electric power as supplied to and harvested from the respective modules of TEM_1 and TEM_2 are described by the symbols of V_{xy1} and V_{xy2}. The lowest and highest magnitude as permitted for the Seebeck coefficient are then represented by the symbols of K_{s1} and K_{s2} with respect to the installed modules of TEM_1 and TEM_2, whilst values of current input are represented by the independent symbols of I_{c1} and I_{c2}.

As observable through the layout in Fig. 3, the segregation of the investigated structure into disparate blocked segments has compellingly defined the affinity between both electrical circuitry and thermal-based models. Such resemblance is exemplified through the analogies between electrical current and heat flow, electrical voltage and temperature, electric conductance and thermal conductivity, electrical capacitance and thermal capacitance, and so forth. With reference to Kirchhoff's law, the TEMs model can be comprehensively understood as

$$C_{d1}\dot{T}_{d1} = G_{da1}T_{a1} - \left(G_{yd1} + G_{da1}\right)T_{d1} + G_{yd1}T_{y1}, \tag{1}$$

$$C_{y1}\dot{T}_{y1} = G_{yd1}T_{d1} + G_{xy1}T_{x1} - \left(G_{xy1} + G_{yd1}\right)T_{y1} + P_{y1}, \tag{2}$$

$$C_{x1}\dot{T}_{x1} = G_{xy1}T_{y1} + G_{xb1}T_b + P_{x1} - \left(G_{xb1} + G_{xy1}\right)T_{x1}, \tag{3}$$

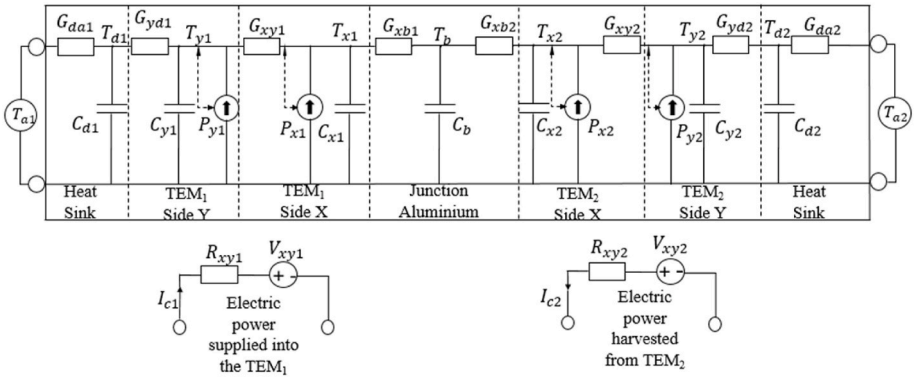

Fig. 3. The given two TEMs model.

$$C_{x2}\dot{T}_{x2} = G_{xb2}T_b + G_{xy2}T_{y2} + P_{x2} - \left(G_{xy2} + G_{xb2}\right)T_{x2}, \tag{4}$$

$$C_{y2}\dot{T}_{y2} = G_{xy2}T_{x2} + G_{yd2}T_{d2} + P_{y2} - \left(G_{yd2} + G_{xy2}\right)T_{y2}, \tag{5}$$

$$C_b\dot{T}_b = G_{xb1}T_{x1} + G_{xb2}T_{x2} - (G_{xb2} + G_{xb1})T_b, \tag{6}$$

$$C_c\dot{T}_c = G_{dc}T_{y2} + G_{ca}T_{a2} - (G_{ca} + G_{dc})T_c, \tag{7}$$

$$C_{d2}\dot{T}_{d2} = G_{yd2}T_{y2} + G_{dc}T_c - \left(G_{yd2} + G_{dc}\right)T_{d2}, \tag{8}$$

where,

$$P_{y1} = I_{c1}^2\frac{R_{xy1}}{2} - K_{s1}T_{y1}I_{c1}, \tag{9}$$

$$P_{x1} = I_{c1}^2\frac{R_{xy1}}{2} + K_{s1}T_{x1}I_{c1}, \tag{10}$$

$$P_{x2} = I_{c2}^2\frac{R_{xy2}}{2} + K_{s2}T_{x2}I_{c2}, \tag{11}$$

$$P_{y2} = I_{c2}^2\frac{R_{xy2}}{2} - K_{s2}T_{y2}I_{c2}, \tag{12}$$

To facilitate the modeling, several key assumptions have been made:

i. **Uniform Excitation Current Input:** It is assumed that the same random excitation current input $\boldsymbol{I_c}$ is used throughout the optimization process across all proposed algorithms. This uniformity is crucial to ensure a fair comparison of the optimization results.
ii. **Parameter Boundaries:** Prior knowledge is utilized to constrain certain parameters within specific boundaries or a physically feasible range. This assumption ensures that the optimization process remains realistic and produces viable parameter estimates.
iii. **Known Model Structure:** The structure of the TEM model, as described in equations (1)–(8), is assumed to be known in advance. This assumption is based on prior knowledge and preliminary experimental investigations, which provide a foundation for the optimization process.
iv. **Steady-State Voltage Assumption**: The voltages of the electric power V_{xy1} and V_{xy2} are assumed to be zero. This assumption is made because only the steady-state relationship is well established, while the theoretical dynamic relationship is not. As a result, this simplification is used to facilitate the modeling process, even though it may limit the accuracy of the model under certain dynamic conditions.

These assumptions are integral to the development and execution of the modeling and optimization processes, defining the context within which the algorithm operates and influencing the interpretation of the results.

2.2. Problem formulation

Parametric identification of TEMs models is especially purposed for diminishing discrepancy between the estimated and the actual models. The block diagram as illustrated towards accurate prediction of the TEMs model has been given in Fig. 4, with input values comprising the data array of I_{c2} and I_{c1}, and T_b and $\widehat{T}_b$ being denoted by I_c, whilst outputs of the actual and the estimated models are individually denoted by T_b and $\widehat{T}_b$. With this in mind, the objective function is ascertained through the value of root mean square error (RMSE), as interpreted by

$$J(\theta) = \sqrt{\frac{1}{N}\sum_{i=1}^{N}(T_b - \widehat{T}_b)^2}\quad . \tag{13}$$

With reference to Equation (13), the 21 identifiable parameters of TEMs model are exclusively represented by vector θ. It can be further extended as $\theta = \left[G_{da1}\ C_{d1}\ G_{yd1}\ C_{y1}\ R_{xy1}\quad k_{s1}\ G_{xy1}\ C_{x1}\ G_{xb1}\ C_b\ G_{xb2}\ C_{x2}\ R_{xy2}\ k_{s2}\ G_{xy2}\ C_{y2}\ G_{yd2}\ C_{d2}\ G_{dc}\ G_{ca}\ C_c\right]^T$. As such, the estimation problem as determined for TEMs model is, therefore, devised by:

Problem 2.1: Retrieve the values of unknown parameters θ that minimize the objective function J of Equation (13) pertaining to the given actual input data of I_{c1} and I_{c2}, and output data of T_b.

3. The original SMA

Initially published in Ref. [22], SMA has been especially galvanized by the oscillating patterns of slime mould towards achieving the desired route of food foraging through appropriated exploratory capability and exploitative proficiency. Replicating the generative technique of positive and negative reactions concerning propagation wave as bolstered by the bio-oscillator, accommodative weights are, therefore, adopted towards development of such contemporary arithmetical model. The revised equation of individual slime mould which mirrors the odor

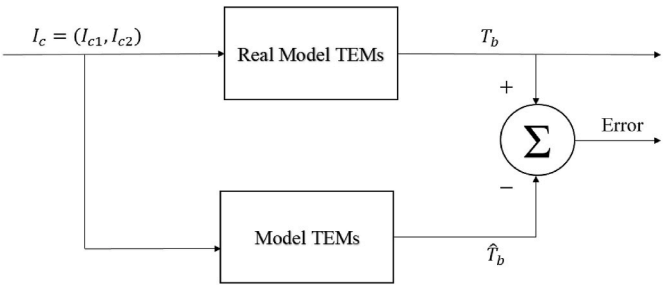

Fig. 4. Block diagram of TEMs Model.

concentration is then described by

$$\tilde{z}_j(t+1) = \begin{cases} r_1 * (ub - lb) + lb, & if \quad r_2 < \beta, \\ \tilde{z}_{bj} + v_b * \left(w * \tilde{z}_{Aj}(t) - \tilde{z}_{Bj}(t)\right), & if \quad r_3 < p \; AND \; r_2 \geq \beta, \\ v_c * \tilde{z}_j(t), & if \quad r_3 \geq p \; AND \; r_2 \geq \beta, \end{cases} \tag{14}$$

for iteration $t = 1, 2, \ldots, t_{max}$, with the maximum iteration being represented by t_{max}. Revisiting the layout of Equation (8), element for position vector $\tilde{z}$ of the slime mould has been disposed by the symbol $\tilde{z}_j$, with element for position vector $\tilde{z}_b$ which identifies the utmost odor concentration located thus far being disposed by the symbol $\tilde{z}_{bj}$. Elements for $\tilde{z}_A$ and $\tilde{z}_B$ which resides arbitrarily nominated individual position vectors of the slime mould are further denoted by the respective symbols of $\tilde{z}_{Aj}$ and $\tilde{z}_{Bj}$. The symbol d is then used to represent dimension for the position vectors of $\tilde{z}$, $\tilde{z}_b$, $\tilde{z}_A$ and $\tilde{z}_B$. Meanwhile, random numbers as separately yielded within the range of [0, 1] have been denoted by the symbols of r_1, r_2, and r_3, with values of the upper and lower bounds being denoted by the respective symbols of ub and lb at a pre-established coefficient of β. A parameter within the range of $[-a, a]$ is concurrently defined by the notation v_b, with the value of a being described by

$$a = \operatorname{arctanh}(1 - (t / t_{max})). \tag{15}$$

Additionally, the notation v_c given in Equation (14) specifies an arbitrary value as selected between an initial range of $[-1, 1]$ which progressively diminishes towards the zero value. The term as demonstrated by p is subsequently defined by

$$p = \tanh|S(i) - DF|, \tag{16}$$

where fitness for individual position vector of the slime mould $\tilde{z}$ at a population size of n is given by $S(i)(i = 1, 2, \ldots, n)$, with the best fitness being represented by DF. Notation w, which is used to signify the slime mould's weight, is then determined based on

$$w(SmellIndex(i)) = \begin{cases} 1 + r_4 * \log\left(\dfrac{BF - S(i)}{BF - WF} + 1\right), & i \in FH, \\ 1 - r_4 * \log\left(\dfrac{BF - S(i)}{BF - WF} - 1\right), & \text{others}, \end{cases} \tag{17}$$

where $SmellIndex$ is incorporated as a function which devised $S(i)$ by orderly disposition of the current iteration initializing the best BF to the worst WF fitness, whilst the first quarter of the hierarchical population corresponded by FH, with an arbitrary value within the range of [0, 1] as manifested by the symbol r_4.

Weight w in Equation (17) notably explains the correlation between food concentration and the thickness of the vein. A proportional relationship is established between both weight and food concentration, in which a higher level of food concentration advocates increased weight of the surroundings, and vice versa. A circumstance where low food concentration encourages greater foraging pursuits towards other territories, thus, enabling swifter allocation of destination with higher food concentration by the slimes. A comparatively sluggish process ensues should the destination hold a lower food concentration. Following increased prospects in acquiring more profound food owing to robust avoidance of the local optima, such a mechanism inevitably elevates the efficiency in determining an optimal level of food source. This is, nonetheless, on accounts where environmental setbacks such as dehydrated surroundings and overwhelming brightness would hinder the circulation of the slime mould.

As such, the pseudocode for the standard SMA has been systematically outlined as per **Algorithm 1**.

Algorithm 1: Pseudocode of the original SMA

1. The population size n, coefficient β, and t_{max} are initially identified. Following this, individual position of the slime mould is arbitrarily executed between the predetermined range of ub and lb.
2. **While** ($t \leq t_{max}$)
3. Fitness of the slime mould is collectively determined
4. The value of w is calculated based on Equation (17)
5. DF and its corresponding $\tilde{z}_b$ are revised and updated
6. The value of a is calculated by employment of Equation (15)
   For each slime mould
7. p, v_b, v_c are revised and updated
8. Individual position of the slime is updated by computation of Equation (14)
9. **End For**
10. $t = t + 1$
11. **End While**
12. **Return** DF and $\tilde{z}_b$

4. Proposed enhanced SMA (ESMA)

In light of the robustness of standard SMA towards resolving issues concerning system optimization, its excellence is situationally demoted by encountered setbacks of local optima entrapment. Preliminary experimentations, nonetheless, uncovered two main antecedents that contribute to such discrepancy. The first reason is recognized in the common revision of the slime mould's location in accordance with the best individual position with the highest odor concentration for every iteration thus far. Failure of the best individual position to escape the local optima would expediently guide surrounding slimes towards a similarly trapped circumstance. Accounting for the extreme disparity between individual and best fitness of the slimes that develops an immense reliance by their respective individual position on the best individual position, the second reason then highlights the ineffective layout of the formula p from Equation (16) in devising sufficient selections and alternatives towards steering the locational update of each slime.

Two disparate alterations are subsequently introduced within the current paper to overcome the aforementioned shortcomings. The primary alteration especially concerns the computation of random average position between both the slimes' current individual position and best individual position for its latest iteration. Superseding the entirety of the simulated iterations, such a proposition is set to enhance the tendency of otherwise trapped slimes to escape the local optima region. Unveiled benefit, therefore, encloses reciprocated supports between the slimes' current individual position and their entrapped best individual position towards the withdrawal of the latter from the local optima region in continuing its contemporary exploration. A visualized representation by the employment of a two-dimensional design parameter ($d = 2$) as set within a pre-established contour plot is further illustrated in Fig. 5 to enable increased clarification of such conditions. Supposition transpires unexpected entrapment of the best individual position $\tilde{z}_b$ (green diamond) within the local optima region. The possibility of $\tilde{z}_b$ in withdrawing from its entangled position is exceptionally high by the implementation of the standard SMA, with the immense tendency of

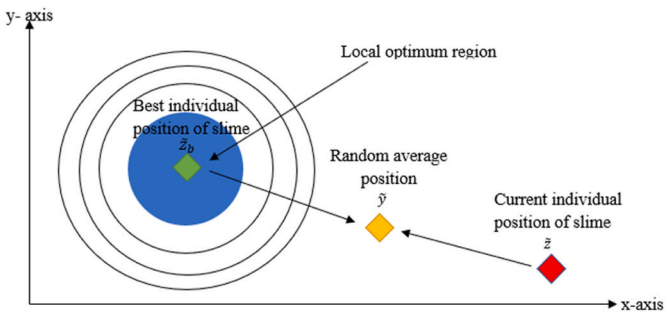

Fig. 5. Graphical representation of the random average position.

dragging its surrounding current individual position of slime $\widetilde{z}$ (red diamond) towards a similar regional mishap. However, such an issue is deemed solvable in the case where the random average position is operationalized based on

$$\widetilde{y}_j = \widetilde{z}_{bj} * r_5 + \widetilde{z}_j * (1 - r_5), \tag{18}$$

as represented by the element of the vector $\widetilde{y}$ (designated using the yellow diamond), with r_5 from Equation (18) being arbitrary values within the range of [0, 1] that have been independently generated.

Thereafter, the second alteration as adopted for this study confronts substitution of tangent hyperbolic function within the existing formula p from Equation (16) with an exponential function towards inducing vaster probable variations for the selection of revised equations in Equation (14). The reworked formula following incorporation of the aforementioned adjustment is then given by

$$\widehat{p} = \exp(-|S(i) - DF|). \tag{19}$$

The revised equation for individual slime as finalized upon the arithmetic layouts given in Equations (18) and (19) is, therefore, described as

$$\widetilde{z}_j(t+1) = \begin{cases} r_1 * (ub - lb) + lb, & \text{if} \quad r_2 < \beta, \\ \widetilde{y}_j + v_b * \left(w * \widetilde{z}_{Aj}(t) - \widetilde{z}_{Bj}(t)\right), & \text{if} \quad r_3 < \widehat{p}\ AND\ r_2 \geq \beta, , \\ v_c * \widetilde{z}_j(t), & \text{if} \quad r_3 \geq \widehat{p}\ AND\ r_2 \geq \beta. \end{cases} \tag{20}$$

Ensuing the pair of operationalized alterations as discussed above, resolution towards overwhelming reliance of the slime's revised individual position on the best individual position is, therefore, anticipated. The effectiveness of these modifications is justified by their ability to address the key limitations identified in the standard SMA. By incorporating a more flexible position update mechanism and reducing reliance on potentially misleading best individual positions, ESMA enhances the algorithm's robustness and performance in optimizing system parameters. The improvements introduced in ESMA have been validated through extensive simulations and comparisons with other optimization algorithms, demonstrating its superior performance in parameter identification for TEMs. The enhancements not only address the issues of local optima entrapment but also provide a more effective and efficient optimization approach. Nevertheless, enhanced SMA (ESMA) is forwarded in advancement to the standard SMA coinciding the contemporary equation as updated in Equation (20). As such, the pseudocode for ESMA is further detailed in **Algorithm 2**.

Algorithm 2: Pseudocode of the proposed ESMA

1. The population size n, coefficient β, and t_{max} are initially identified. Following this, individual position of the slime mould is arbitrarily executed between the predetermined range of ub and lb.
2. **While** ($t \leq t_{max}$)
3. Fitness of the slime mould is collectively determined
4. The value of w is computed based on Equation (17)
5. DF and it's corresponding $\widetilde{z}_b$ are revised and updated
6. The value of a is computed by the employment of Equation (15)
   For each slime mould
7. $\widehat{p}, \widetilde{y}, v_b, v_c$ are revised and updated
8. Individual position of the slime is revised by computation of Equation (20)
9. **End For**
10. $t = t + 1$
11. **End While**
12. **Return** DF and $\widetilde{z}_b$

Despite the modifications in Equations (19) and (20), the complexity of the proposed ESMA still remains the same as the original SMA. Specifically, based on the population size n, maximum iterations t_{max} and size of dimension d, the computational complexity for initialization is $O(d)$, and for fitness evaluation and sorting, it is $O(n + n \log n)$. The complexity of updating the weight and position is both $O(n \times d)$. In summary, the overall computational complexity of the proposed ESMA is represented by $O(d + nt_{max}(1 + \log n + d))$. Please refer to Ref. [39] for the details.

Nevertheless, the structured procedure for the implementation of ESMA within a TEMs model is manifested upon.

Step 1. Previously unidentified parameters θ of the TEMs model are determined in accordance with the mathematical model as outlined in Section 2.

Step 2. The proposed ESMA-based approach is operationalized conforming to **Algorithm 2** by establishing $\theta := \widetilde{z}$ and $J(\theta) = S(i)$ towards individual slime mould.

Step 3. Algorithmic operation is discontinued upon reaching the maximum iterations t_{max}, whilst the best individual position of the slime $\widetilde{z}_b$ being defined as the optimal parameter of the TEMs model, $\theta := \widetilde{z}_b$.

5. Results and discussion

This section is developed to appraise the performance of TEMs Model based on the implemented parametric optimization of ESMA based method. The effectiveness of the proposed method is consequently benchmarked against performances of the standard SMA, as well as other preceding algorithms such as PSO [19], GWO, BES, and MFO-based methods, with respect to the criteria described as follows:

1. Evaluation towards the convergence curve of the average objective function as obtained through 20 trials, followed by the appraisal of the parameter deviation index ξ. As such, the parameter deviation index as assessed based on 21 estimated parameters of the TEMs model is computed by

$$\xi = \left\| \frac{\theta_1 - \widehat{\theta}_1}{\widehat{\theta}_1}, \ldots, \frac{\theta_{21} - \widehat{\theta}_{21}}{\widehat{\theta}_{21}} \right\|_2 \tag{21}$$

where $\widehat{\theta} \in R^{21}$, the ith component for the given design parameter vector $\widehat{\theta}$ is represented by $\widehat{\theta}_i$, with the ith component for the ascertained design parameter θ being further represented by θ_i.

2. Analysis enclosing the statistical yields for both fitness function and parameter deviation index through 20 separate trials pertaining to the calculated values of mean, best, worst and standard deviation (Std.) among the currently examined ESMA, SMA, PSO [19], GWO, BES, and MFO based methods.

Experimented simulations were comprehensively attempted via MATLAB of a laptop equipping the specifications of Intel(R) Core (TM) i3-7020U CPU @ 2.30 GHz, 12 GB RAM and Windows 10 system. At a pre-established coefficient β of 0.61, performances of the proposed ESMA and the standard SMA-based methods were measured against other existing optimization approaches such as PSO [19], GWO, BES, and MFO based methods at their corresponding coefficients as tabulated in Table 1. Identical regulatory principles were particularly identified for the entirety of the examined algorithms throughout the simulations to ensure unbiased comparability, following the criteria of $n = 20$, $t_{max} = 50$, as well as the upper and lower boundaries as specified in Table 1. 20 separate trials were then executed to uniformly calibrate the recorded outcomes of ESMA based method against performances of its predecessors. Appropriating to the block diagram as presented in Fig. 4, both the input signals I_{c1} and I_{c2}, and the output signal T_b which acted as reference points for parametric identification of the proposed algorithm within the TEMs model have, thus, been independently plotted in Fig. 6 (a), (b) and 6(c), respectively.

The convergence curves of the best fitness function, obtained from 20 independent trials, are presented in Fig. 7 for the algorithms based on ESMA, SMA, PSO [19], GWO, BES, and MFO. The results of the proposed

Table 1
Comparison among parameter estimation of algorithms.

Algorithm	Real Model	*lb*	*ub*	ESMA	SMA	PSO [19]	GWO	BES	MFO
G_{da1} (W /K)	10	5	20	9.89	6.11	5	13.42	9.51	5.46
C_{d1} (J /K)	3500	3000	4000	3289.18	3898.75	3850.15	3222.16	3000.13	3000.73
G_{yd1} (W /K)	24	20	30	20.00	20	20	25.78	25.28	22.15
C_{y1} (J /K)	108	105	110	105.44	107.76	110	110	105.05	105.46
R_{xy1} (Ω)	1.32	1	5	1.49	1.79	1.56	2.16	1.52	1.11
k_{s1} (V /K)	0.02	0.01	0.04	0.02	0.02	0.02	0.02	0.02	0.02
G_{xy1} (W /K)	0.23	0.1	0.5	0.25	0.33	0.14	0.14	0.21	0.27
C_{x1} (J /K)	3.2	3	4	3.37	3.7	3	3.13	3.95	3.00
G_{xb1} (W /K)	10	5	30	9.65	7.09	21.92	5.42	5.11	13.45
C_b (J /K)	42.75	20	60	37.81	48.22	40.45	45.86	43.01	48.08
G_{xb2} (W /K)	10	5	30	5.18	7.14	7.45	6.85	5.05	20.43
C_{x2} (J /K)	3.2	3	4	3.05	3.77	4	3.01	3.61	3.05
R_{xy2} (Ω)	1.32	1	5	1.59	1.75	1	1.63	1.00	2.41
k_{s2} (V /K)	0.02	0.01	0.04	0.02	0.02	0.02	0.02	0.02	0.02
G_{xy2} (W /K)	0.23	0.1	0.5	0.18	0.22	0.31	0.40	0.28	0.26
C_{y2} (J /K)	108	105	110	105.00	108.85	105	108.12	105.05	109.93
G_{yd2} (W /K)	24	20	30	21.79	21.82	20.15	21.97	28.58	24.59
C_{d2} (J /K)	3500	3000	4000	3123.21	3493.37	3002.17	4000	3908.34	3630.94
G_{dc} (W /K)	10	5	20	7.61	5.15	11.78	6.41	14.74	19.99
G_{ca} (W /K)	10	5	20	8.53	8.58	5.19	8.01	5.05	15.59
C_c (J /K)	3500	3000	4000	3249.80	3606.53	3000	3234.69	3919.64	3692.81
			Best ξ	0.74	1.07	1.59	1.35	1.12	1.88

ESMA-based method are represented by the green line, while the outcomes of the SMA, PSO, GWO, BES, and MFO algorithms are depicted by the yellow, blue, magenta, cyan, and black lines, respectively. The figure demonstrates that, during the initial iterations, the ESMA, GWO, MFO and BES algorithms achieve faster convergence compared to the original SMA and PSO algorithms, highlighting their effectiveness in the exploration phase. Towards the end of the maximum iterations, ESMA continues to improve its fitness function, resulting in the lowest fitness function among the algorithms. This convergence curve also validates the effectiveness of the proposed random average position in the ESMA update equation in avoiding local entrapment issues.

In addition, the computational time results are utilized to evaluate the computational complexity, revealing that the proposed ESMA and the SMA have average execution times of 137.0973 min and 137.7354 min, respectively, over 20 trials. This indicates that the modifications introduced in Equations (19) and (20) within the ESMA framework do not contribute to a significant increase in computational complexity compared to the original SMA. Acquired results, therefore, endorsed the superiority of ESMA based method in generating the best performance for the majority of the fitness function over other well-established optimization approaches throughout the progression of the simulated iterations. Further bolstered by the finest design parameters as determined through 20 individual trials and their respective parameter deviation index ξ, recorded values as tabulated in Table 1 then confirmed the closest proximity between results by the implementation of ESMA based method and the given parameters of an actual model over its predecessors, whilst having the lowest parameter deviation index ξ of 0.6401. With following a hierarchical order of SMA, BES, GWO, PSO [19] and MFO-based methods, their performances have, nonetheless, been significantly outshined by the proposed method.

Moreover, statistical fitness function outcomes of the examined algorithms with respect to the values of best, mean, worst and standard deviation as recorded from 20 individually simulated trials are comprehensively outlined in Table 2. The results indicate that the ESMA-based method exhibits the lowest values for the best, worst, and standard deviation of the fitness function, with mean values that are slightly competitive with those of the GWO and BES methods. This further demonstrates the effectiveness of the proposed approach compared to the alternative algorithms. Likewise, such findings are reflected through the parameter deviation index which coheres to the evaluation of best, mean, worst and standard deviation values as presented in Table 3. The cumulative findings indicate that the ESMA-based method consistently outperforms in minimizing the best, mean, worst, and standard deviation values of the parameter deviation index ξ. In contrast, despite achieving lower RMSE values, the GWO and BES-based methods struggle to produce a superior parameter deviation index.

The outcomes for both actual temperature output T_b and estimated temperature output $\widehat{T}_b$ of the examined algorithms are consequently outlined in Fig. 8. Performance of the actual model is hereby plotted using a black colored line, with the streamlined algorithms comprising ESMA, SMA and PSO [19] based methods being further plotted using the green, yellow and blue colored lines, respectively. Having the finest parametric estimation in Table 1 as a basis for the acquired results of estimated temperature output T_b, specific zoomed domains as demonstrated in Fig. 8, thus, showcasing an identifiable resemblance between responses of the ESMA-based method and the actual output signal. Such a claim is further substantiated by a diminished error response of the proposed approach in Fig. 9, as compared to the standard SMA and PSO [19] based counterparts. Aggregated responses have undeniably corroborated ESMA as the superior alternative over performances of the standard SMA and PSO [19] based methods towards precise identification of the TEMs model.

6. Conclusion

ESMA has been specially introduced in the current paper as a contemporarily enhanced variant of SMA for the fine-tuning of the TEMs model. A hybridized approach between two different techniques; such algorithm sets to resolve the shortcomings of its predecessor with accounts for random average position between the slimes' current individual position and finest individual position in overcoming the issue of local optima entrapment, alongside substitution of an exponential function to the existing tangent hyperbolic function for formula p of the standard SMA in accrediting increasingly diversified alternatives on the selection of revised equations. The robustness of the proposed algorithm was inherently validated upon its proficiency in optimizing the parameters of a TEMs model.

Undertaken simulations further demonstrated the relative supremacy of the ESMA-based approach against former optimization alternatives including the standard SMA, PSO [19], GWO, BES, and MFO, in terms of RMSE values throughout the majority of the experimented trials. Increased model accuracy was similarly achieved by the proposed approach over its compared algorithms with respect to the parameter

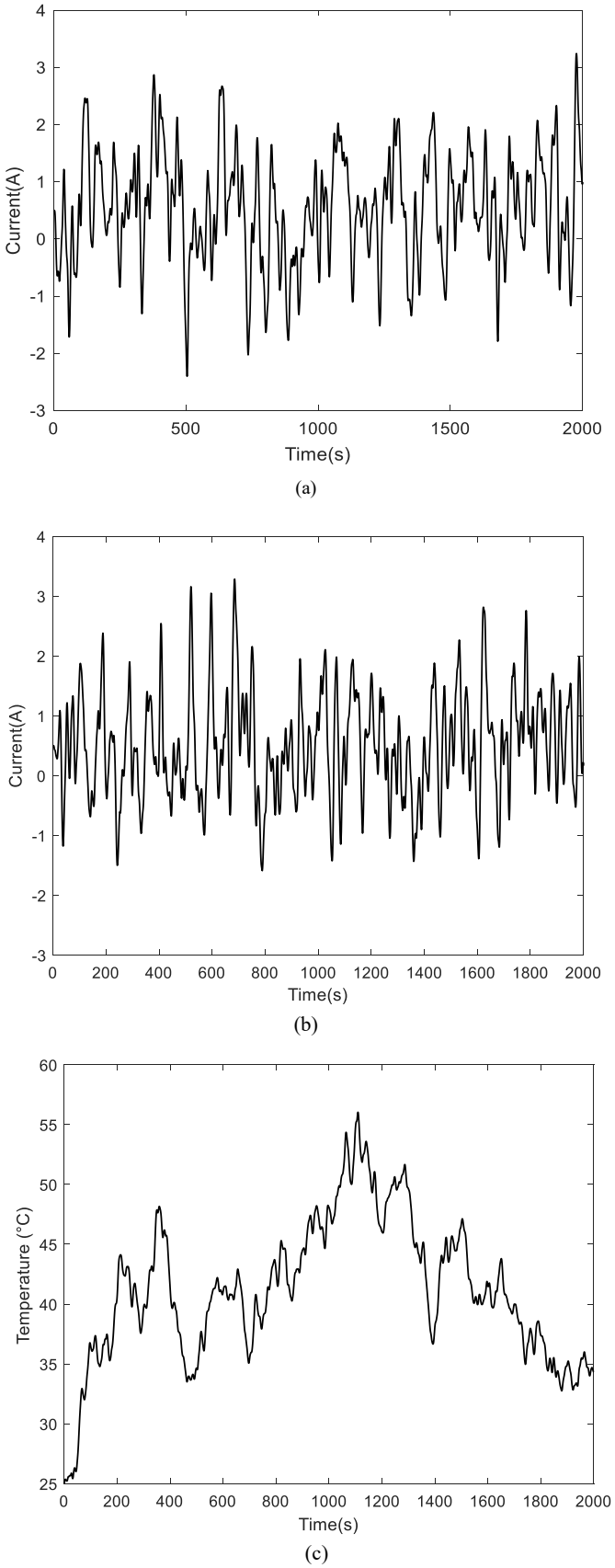

Fig. 6. (a) Input signal of I_{c1}; (b) Input signal of I_{c2} (c) Output signal of T_b.

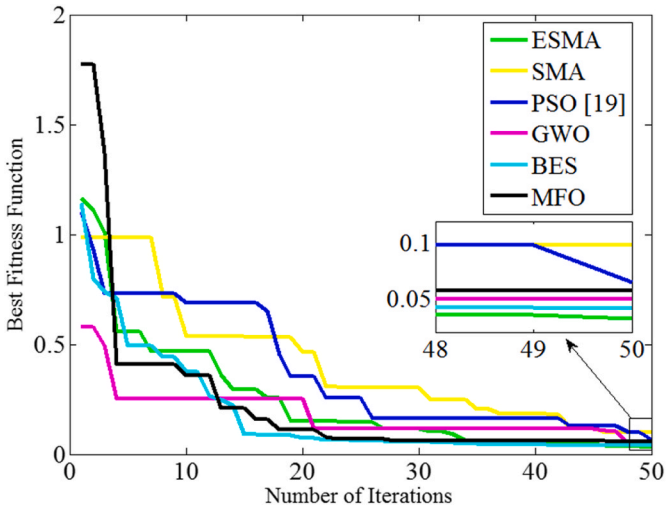

Fig. 7. The convergence curve of the best fitness function from 20 trials.

Table 2
The statistical performance value of the RMSE.

Algorithm	ESMA	SMA	PSO [19]	GWO	BES	MFO
Best	**0.0321**	0.09843	0.0649	0.0498	0.0417	0.0578
Mean	0.1627	0.1802	0.2079	**0.1503**	0.1544	0.1684
Worst	**0.2001**	0.29022	0.5292	0.3289	0.3211	0.3012
Standard	**0.0455**	0.0521	0.1135	0.0605	0.0708	0.0713

deviation index between the actual and the estimated design parameters. Transcending competencies of earlier algorithms in securing the utmost optimal parameters to a TEMs model, the far-reaching potential of the contemporary approach as an excellent optimizer is, therefore, recognized.

However, despite the promising results, several limitations of the ESMA approach should be acknowledged. One of the primary limitations is the high computational time, which is largely due to the large population size required for the algorithm's operation. This could pose a challenge when applying ESMA to real-time control engineering problems. Future research could explore the effectiveness of ESMA with a smaller or dynamically adjusted population size to mitigate this issue. Additionally, the scalability of ESMA to more complex and synthesized systems remain to be validated. Upcoming studies should focus on applying ESMA to a wider range of systems to confirm its real-time operational applicability. Overall, while ESMA has proven to be a highly effective and precise mechanism in system modeling, addressing its limitations in future work will be essential to fully harness its potential in real-world applications.

CRediT authorship contribution statement

Dharswini Ponnalagu: Writing – original draft, Validation, Methodology, Data curation. **Mohd Ashraf Ahmad:** Writing – review & editing, Supervision, Conceptualization. **Julakha Jahan Jui:** Writing – review & editing, Investigation, Formal analysis.

Declaration of competing interest

The authors declare the following financial interests/personal relationships which may be considered as potential competing interests: Mohd Ashraf Ahmad reports financial support was provided by University of Malaysia Pahang Al-Sultan Abdullah. If there are other authors, they declare that they have no known competing financial interests or personal relationships that could have appeared to influence

Table 3
The statistical performance value of the parameter deviation, ξ.

Algorithm	ESMA	SMA	PSO [19]	GWO	BES	MFO
Best	**0.73589**	1.07186	1.58811	1.35003	1.11628	1.88196
Mean	**1.27917**	1.83643	2.83876	2.02806	1.56745	2.43273
Worst	**1.61763**	2.76139	3.90609	2.91367	2.23111	3.71352
Standard	**0.30527**	0.44091	0.57210	0.48757	0.32113	0.43593

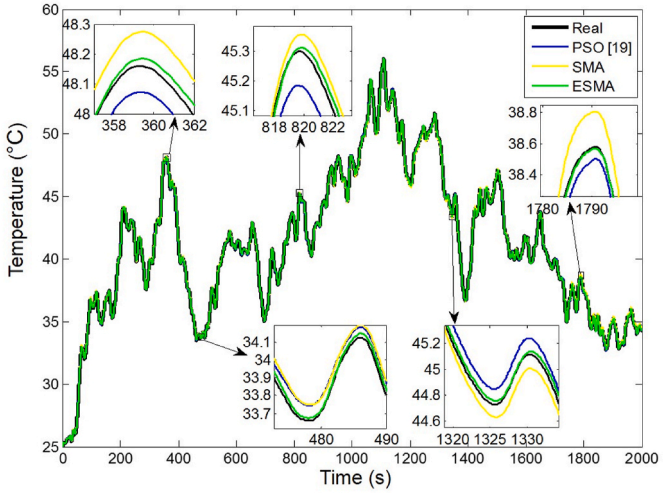

Fig. 8. Comparison of output signal T_b.

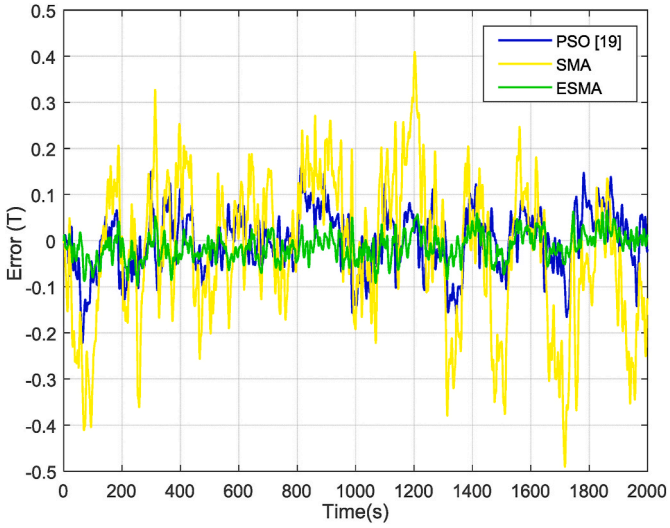

Fig. 9. Signal error between T_b and $\widehat{T}_b$.

the work reported in this paper.

Data availability

Data will be made available on request.

Acknowledgments

This paper acknowledges Universiti Malaysia Pahang Al-Sultan Abdullah for funding our research through the Distinguished Research Grant Scheme (University Ref. No. RDU223011).

References

[1] A. Sánchez-Roncero, Ò. Garibo-i-Orts, J.A. Conejero, H. Eivazi, F. Mallor, E. Rosenberg, F. Fuso-Nerini, J. García-Martínez, R. Vinuesa, S. Hoyas, The sustainable development goals and aerospace engineering: a critical note through artificial intelligence, Results in Engineering 17 (2023) 100940, https://doi.org/10.1016/j.rineng.2023.100940.

[2] Y. Xie, S.J. Wu, C.J. Yang, A thermoelectric cap for seafloor hydrothermal vents, Energy Convers. Manag. 109 (2016) 166–174, https://doi.org/10.1016/j.enconman.2015.12.003.

[3] A. Dewan, S.U. Ay, M.N. Karim, H. Beyenal, Alternative power sources for remote sensors: a review, J. Power Sources 245 (2014) 129–143, https://doi.org/10.1016/j.jpowsour.2013.06.081.

[4] V. Leonov, T. Torfs, P. Fiorini, C. Van Hoof, Thermoelectric converters of human warmth for self-powered wireless sensor nodes, IEEE Sensor. J. 7 (5) (2007) 650–656, https://doi.org/10.1109/JSEN.2007.894917.

[5] C. McWebb, University of alberta, Florilegium 20 (1) (2003) 59–61, https://doi.org/10.3138/flor.20.015.

[6] J. Jiang, System Modeling and Controller Designs for a Peltier-Based Thermal Device in Microfluidic Application, 2010. Doctoral Dissertation.

[7] S. Petryna, Model Predictive Control of a Thermoelectric-Based Heat Pump, 2013. Doctoral Dissertation.

[8] K.L. Grosse, M.H. Bae, F. Lian, E. Pop, W.P. King, Nanoscale Joule heating, Peltier cooling and current crowding at graphene-metal contacts, Nat. Nanotechnol. 6 (5) (2011) 287–290, https://doi.org/10.1038/nnano.2011.39.

[9] A.H. Nayfeh, B. Balachandran, Chapter 6: numerical methods, Appl. Nonlinear Dyn. (2004) 423–460, https://doi.org/10.1002/9783527617548 [Online]. Available:.

[10] M. Kober, Holistic development of thermoelectric generators for automotive applications, J. Electron. Mater. 49 (5) (2020) 2910–2919, https://doi.org/10.1007/s11664-020-07966-6.

[11] R. Sok, J. Kusaka, Development and validation of thermal performances in a novel thermoelectric generator model for automotive waste heat recovery systems, Int. J. Heat Mass Tran. 202 (2023) 123718, https://doi.org/10.1016/j.ijheatmasstransfer.2022.123718.

[12] M.S.B. Dzulkfli, A. Pesyridis, D. Gohil, Thermoelectric generation in hybrid electric vehicles, Energies 13 (14) (2020) 3742, https://doi.org/10.3390/en13143742.

[13] T. Kousksou, J.-P. Bédécarrats, D. Champier, P. Pignolet, C. Brillet, Numerical study of thermoelectric power generation for an helicopter conical nozzle, J. Power Sources 196 (2011) 4026–4032, https://doi.org/10.1016/j.jpowsour.2010.12.015.

[14] S. Usón, J. Royo, P. Canalís, Integration of thermoelectric generators in a biomass boiler: experimental tests and study of ash deposition effect, Renew. Energy 214 (2023) 395–406, https://doi.org/10.1016/j.renene.2023.05.100.

[15] W. Moser, G. Friedl, W. Haslinger, H. Hofbauer, Small-scale pellet boiler with thermoelectric generator, in: 25th International Conference on Thermoelectrics, 2006, pp. 349–353, https://doi.org/10.1109/ICT.2006.331221.

[16] N.R. Kristiansen, G.J. Snyder, H.K. Nielsen, L. Rosendahl, Waste heat recovery from a marine waste incinerator using a thermoelectric generator, J. Electron. Mater. 41 (2012) 1024–1029, https://doi.org/10.1007/s11664-012-2009-6.

[17] K. Yazawa, A. Shakouri, T.J. Hendricks, Thermoelectric heat recovery from glass melt processes, Energy 118 (2017) 1035–1043, https://doi.org/10.1016/j.energy.2016.10.136.

[18] M. Alnajideen, G. Min, Hybrid photovoltaic-thermoelectric system using a novel spectral splitting solar concentrator, Energy Convers. Manag. 251 (2022) 114981, https://doi.org/10.1016/j.enconman.2021.114981.

[19] D.R. Ojeda G, L.A.L. de Almeida, O.A.C. Vilcanqui, Parameter estimation of nonlinear thermoelectric structures using particle swarm optimization, Simulat. Model. Pract. Theor. 81 (2018) 1–10, https://doi.org/10.1016/j.simpat.2017.11.004.

[20] L.A. de Almeida, O.A. Vilcanqui, Parameter identification of thermoeletric modules using particle swarm optimization. IEEE International Instrumentation and Measurement Technology Conference (I2MTC), 2015, pp. 812–817, https://doi.org/10.1109/I2MTC.2015.7151373.

[21] M. Allyson-Cyr, L. Gosselin, Comparison between five stochastic global search algorithms for optimizing thermoelectric generator designs, Numer. Heat Tran., Part A: Applications 76 (5) (2019) 323–347, https://doi.org/10.1080/10407782.2019.1630241.

[22] S. Li, H. Chen, M. Wang, A.A. Heidari, S. Mirjalili, Slime mould algorithm: a new method for stochastic optimization, Future Generat. Comput. Syst. 111 (2020) 300–323, https://doi.org/10.1016/j.future.2020.03.055.

[23] C. Kumar, T.D. Raj, M. Premkumar, T.D. Raj, A new stochastic slime mould optimization algorithm for the estimation of solar photovoltaic cell parameters, Optik 223 (August) (2020) 165277, https://doi.org/10.1016/j.ijleo.2020.165277.

[24] M. Abdel-Basset, V. Chang, R. Mohamed, HSMA_WOA: a hybrid novel Slime mould algorithm with whale optimization algorithm for tackling the image segmentation problem of chest X-ray images, Appl. Soft Comput. J. 95 (2020) 106642, https://doi.org/10.1016/j.asoc.2020.106642.
[25] S. Ekinci, D. Izci, H.L. Zeynelgil, S. Orenc, An application of slime mould algorithm for optimizing parameters of power system stabilizer, in: 4th Int. Symp. Multidiscip. Stud. Innov. Technol. ISMSIT 2020 - Proc., 2020, pp. 1–5, https://doi.org/10.1109/ISMSIT50672.2020.9254597.
[26] Z. Chen, W. Liu, An efficient parameter adaptive support vector regression using K-Means clustering and chaotic slime mould algorithm, IEEE Access 8 (2020) 156851–156862, https://doi.org/10.1109/ACCESS.2020.3018866.
[27] S. Mirjalili, S.M. Mirjalili, A. Lewis, Grey wolf optimizer, Adv. Eng. Software 69 (2014) 46–61, https://doi.org/10.1016/j.advengsoft.2013.12.007.
[28] H.A. Alsattar, A.A. Zaidan, B.B. Zaidan, Novel meta-heuristic bald eagle search optimisation algorithm, Artif. Intell. Rev. 53 (2020) 2237–2264, https://doi.org/10.1007/s10462-019-09732-5.
[29] S. Mirjalili, Moth-flame optimization algorithm: a novel nature-inspired heuristic paradigm, Knowl. Base Syst. 89 (2015) 228–249, https://doi.org/10.1016/j.knosys.2015.07.006.
[30] A.A. Bhandakkar, L. Mathew, Merging slime mould with whale optimization algorithm for optimal allocation of hybrid power flow controller in power system, J. Exp. Theor. Artif. Intell. 35 (7) (2022) 973–1000, https://doi.org/10.1080/0952813X.2022.2040598.
[31] M. Abdel-Basset, V. Chang, R. Mohamed, HSMA_WOA: a hybrid novel Slime mould algorithm with whale optimization algorithm for tackling the image segmentation problem of chest X-ray images, Appl. Soft Comput. 95 (2020) 106642, https://doi.org/10.1016/j.asoc.2020.106642.
[32] C. Zhong, G. Li, Z. Meng, A hybrid teaching–learning slime mould algorithm for global optimization and reliability-based design optimization problems, Neural Comput. Appl. 34 (2022) 16617–16642, https://doi.org/10.1007/s00521-022-07277-3.
[33] T. Kundu, H. Garg, LSMA-TLBO: a hybrid SMA-TLBO algorithm with lévy fight based mutation for numerical optimization and engineering design problems, Adv. Eng. Software 172 (2022) 103185, https://doi.org/10.1016/j.advengsoft.2022.103185.
[34] H. Chen, X. Li, S. Li, Y. Zhao, J. Dong, Improved slime mould algorithm hybridizing chaotic maps and diferential evolution strategy for global optimization, IEEE Access 10 (2022) 66811–66830, https://doi.org/10.1109/ACCESS.2022.3183627.
[35] M.Z. Mohd Tumari, M.A. Ahmad, M.H. Suid, M.R. Ghazali, M.O. Tokhi, An improved marine predators algorithm tuned data-driven multiple-node hormone regulation neuroendocrine-PID controller for multi-input–multi-output gantry crane system, J. Low Freq. Noise Vib. Act. Control 42 (4) (2023) 1543–1936, https://doi.org/10.1177/14613484231183938.
[36] M.Z. Mohd Tumari, M.A. Ahmad, M.H. Suid, M.R. Hao, An improved marine predators algorithm-tuned fractional-order PID controller for automatic voltage regulator system, Fractal and Fractional 7 (7) (2023) 561, https://doi.org/10.3390/fractalfract7070561.
[37] M.H. Suid, M.A. Ahmad, A.N.K. Nasir, M.R. Ghazali, J.J. Jui, Continuous-time hammerstein model identification utilizing hybridization of augmented sine cosine algorithm and game-theoretic approach, Results in Engineering 23 (2024) 1–23, https://doi.org/10.1016/j.rineng.2024.102506.
[38] L. Devarajah, M.A. Ahmad, J.J. Jui, Identifying and estimating solar cell parameters using an enhanced slime mould algorithm, Optik 331 (2024) 1–22, https://doi.org/10.1016/j.ijleo.2024.171890.
[39] F.S. Gharehchopogh, A. Ucan, T. Ibrikci, B. Arasteh, G. Isik, Slime mould algorithm: a comprehensive survey of its variants and applications, Arch. Comput. Methods Eng. 30 (4) (2023) 2683–2723, 10.1007%2Fs11831-023-09883-3.